

Comparative Study on Diagonal Strut Model of Infill Wall

Zhenling Chai¹, Zixiong Guo^{1,*}, Xiaojuan Liu¹ and Yunfan Jiang¹

Abstract: The equivalent diagonal strut models of infill wall mainly include the single strut model and multi-strut model. Firstly, several equivalent strut models and their characteristics are introduced in this paper. Then, model analysis and pushover analysis are carried out on infilled frame models with the aid of the software SAP2000. Two typical single strut models and a typical three-strut model are used to simulate the panel of the frames respectively. It is indicated that the period reduction factor of the frame with a three-strut model is close to the value recommended by the current code. The infill wall has great influence on the overall stiffness, bearing capacity and weak position of the structure. The stiffness and the bearing capacity of the infilled frame increase with the increase of the number of the infill walls. The unfilled story is the weak position of the infilled frame, and when the unfilled story at the bottom of the infilled frame, the seismic response of the upper infill layer decreases with the increasing of the number of unfilled story.

Keywords: Infill wall, equivalent strut model, comparative study, pushover analysis.

1 Introduction

The frame structure is widely used in all over the world because of its characteristics of flexible layout form, light weight and more. Its design methods are considered to be mature [Guo, Huang, Wei et al. (2010)]. However, there are still some problems in the design method of frame structures. For example, infill panels are normally considered to be non-structural components [De, Verderame and Martinez (2014); Tasnimi and Mohebkah (2011); Mehrabi and Shing (2002); Huang (2011)], and most codes only consider the influence of the infill panels on the stiffness of the frame. The influence of the infills on the overall mechanical performance of the frame (e.g. bearing capacity and the position of weak story, etc.) is not considered, which may cause hidden dangers.

In order to take adverse effects of infill walls into account, many scholars have carried out experimental study on the infilled frames [Basha and Kaushik (2016); Chiou and Hwang (2015); Pujol and Fick (2010); Puglisi, Uzcategui and Florez-Lopez (2009)] and have proposed different numerical models to simulate the mechanical behavior of the infill walls. In general, there are two types of numerical models: Micro-model [Asteris, Cotsovos, Chrysostomou et al. (2013); Moaveni, Stavridis, Lombaert et al. (2013); Yuen and Kuang (2015); Koutromanos, Stavridis, Shing et al. (2011)] and macro-model [Furtado, Rodrigues and Arede (2015); Moretti, Mousafiroopoulos, Fotakopoulos et al. (2013); Karayannis and Favvate (2011); Furtado, Rodrigues, Arede et al. (2015);

¹ College of Civil Engineering, Huaqiao University, Xiamen, 361021, China.

* Corresponding Author: Zixiong Guo. E-mail: guozxcy@hqu.edu.cn.

Mulgund and Kulkarni (2011); Fiore, Netti and Monaco (2012); EI-Dakhakhni, Elgaaly and Hamid (2003); Cavaleri and Trapani (2014); Crisafulli, Carr and Park (2000)]. Micro-model is first proposed by Mallick and Severn [Mallick and Severn (1967)]. The model simulates the brick block by continuous solid element and simulates the mortar by interface element. Although the calculation result of the micro-model is more accurate, and the calculating process is time consuming, which indicates that the model is not applicable to the analysis of the whole structure. The macro model is mainly represented by the equivalent strut model in which the infill wall is replaced by a pressure strut arranged at the diagonal direction of the frame. Due to its high computational efficiency, this model is often used in the analysis of the whole structure.

The main object of this paper is to discuss the accuracy of the current equivalent strut model, and the influence of the infill wall on the infilled frame. Several methods for determining the inclined rod of the model are first introduced in the paper. Then the accuracy of the Tong's model in which the infill wall is simply equivalent to a cantilever beam, FEMA model in which the relative stiffness between the frame and the infill wall is considered, and Saneinejad model in which the interaction between the frame and the infill wall is considered, are evaluated by the modal analysis. Finally, through the pushover analysis of the whole building with equivalent strut model, the influence of the full arrange infill wall (assuming the infill walls are remained in elastic stage during loading) and the irregular configuration of the infilled wall on the mechanical performance of the whole structure is evaluated, which can provide a reference for similar research.

2 Single strut model

The single strut model uses a single diagonal strut with the same material as the infill wall and only bearing pressure to simulate the infill wall. The thickness of the strut is equal to that of the infill wall, and the width of the strut is determined according to the propose strut models. Some typical equivalent strut models are introduced as follow:

- (1) Holmes [Holmes (1961)] suggested that the width of the strut is equal to 1/3 of the diagonal length of the panel:

$$\omega = d/3 \quad (1)$$

where d is the diagonal length of the panel; ω is the equivalent width of the strut.

- (2) Assuming that the infill panel is a cantilever beam [Tong, Qian, Liang et al. (1985)], the stiffness of the panel is composed of bending stiffness and shear stiffness:

$$K_w = \frac{1}{\frac{H_w^3}{3E_w I_w} + \frac{1.2H_w}{G_w A_w}} \quad (2)$$

where K_w is the stiffness of the panel; H_w is the height of the panel; E_w and G_w are young's modulus and shear modulus of the masonry infill respectively; I_w and A_w are the inertia moment and area of the horizontal cross section of the panel. Then the uniaxial compressive stiffness of the strut can be obtained by:

$$K_s = \frac{K_w}{\cos^2 \theta} \quad (3)$$

where θ is the included angle between the diagonal direction and the horizontal direction of the infill. The area of the strut can be obtained by:

$$A_s = \frac{K_s d}{E_w} \quad (4)$$

Though the geometric dimensions and material properties of infill panels are considered in Tong's model, the relative stiffness between the frame and the infill panel is not considered.

(3) Smith [Smith (1966)] considered that the width of strut increases with the increasing of the stiffness ratio between the infilled panel and the infilled panel. The width of the strut can be obtained by:

$$\omega = \frac{\pi}{2\lambda} \quad (5)$$

$$\lambda = 4 \sqrt{\frac{E_w t_w \sin 2\theta}{4E_c I_c H_w}} \quad (6)$$

where E_c and I_c are the young's modulus and the inertia moment of the concrete column respectively, and t_w is the thickness of infill wall.

(4) The strut model adopted in FEMA 273 [FEMA and ASCE (1997)] and FEMA 356 [FEMA and ASCE (2000)] is the most widely used model at present.

$$\omega = 0.175(\lambda H_w)^{-0.4} d \quad (7)$$

where ω can be obtained by formula (6).

3 Two-strut model

Fiore et al. [Fiore, Netti and Monaco (2012)] proposed a nonparallel two-strut model, as shown in Fig. 1, The width of the strut can be obtained by:

$$\frac{\omega}{d} = \kappa \frac{c}{z} \frac{1}{(\lambda^*)^\beta} \quad (8)$$

where

$$\lambda^* = \frac{E_w t_w H_{0w}}{E_f A_c} \left[\left(\frac{H_{0w}}{L_{0w}} \right)^2 + \frac{1}{4} \frac{A_c}{A_b} \frac{L_{0w}}{H_{0w}} \right] \quad (9)$$

$$\kappa = 1 + (18\lambda^* + 200) \varepsilon_v \quad (10)$$

$$\varepsilon_v = \frac{F_v}{2A_c E_f} \quad (11)$$

$$c = 0.249 - 0.0116v + 0.567v^2 \tag{12}$$

$$\beta = 0.146 + 0.0073v + 0.126v^2 \tag{13}$$

$$z = 1 + 0.25 \left(\frac{L_w}{H_w} - 1 \right) \tag{14}$$

where E_F is the young's modulus of frame; ν is Poisson's ratio of infill masonry; A_c and A_b are the areas of column and beam respectively; F_v is the vertical load; L_w is the length of infill wall. The other parameters are shown in Fig. 1.

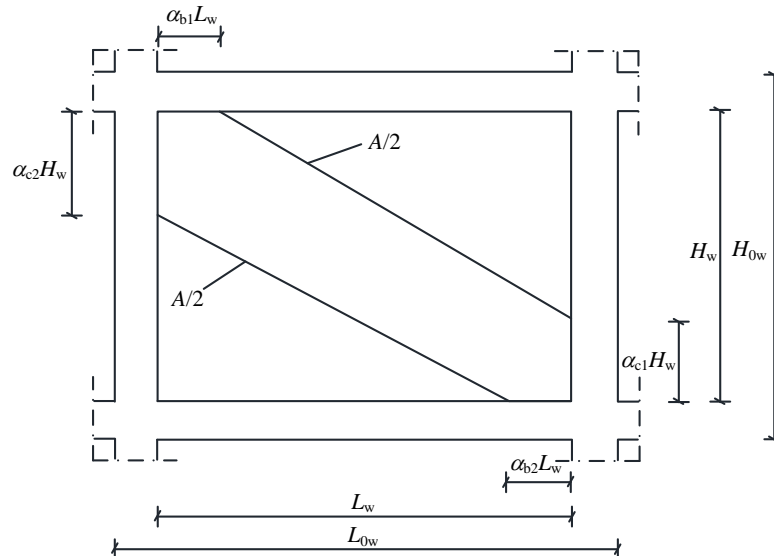


Figure 1: Two-strut model

The contact length between the frame and infill wall is related to the aspect ratio and storey level of the infilled wall.

For the first level, the contact length can be obtained by:

$$\left\{ \begin{array}{l} \alpha_{c1} = 0.10834 \left(\frac{L_w}{H_w} \right)^{-1} + 0.0073141 \left(\frac{L_w}{H_w} \right)^2 \\ 1 - \alpha_{b1} = 0.48689 \left(\frac{L_w}{H_w} \right)^{-2} + 0.16302 \left(\frac{L_w}{H_w} \right)^{0.5} \\ \alpha_{c2} = 0.157621 \left(\frac{L_w}{H_w} \right)^{-1} + 0.084484 \left(\frac{L_w}{H_w} \right)^{0.5} \\ 1 - \alpha_{b2} = 0.408621 \left(\frac{L_w}{H_w} \right)^{-0.5} + 0.44431 \left(\frac{L_w}{H_w} \right)^{0.5} \end{array} \right. \tag{15}$$

For the upper level, the contact length can be obtained by:

$$\left\{ \begin{array}{l} \alpha_{c1} = 0.11609 \left(\frac{L_w}{H_w} \right)^{-1} + 0.0061624 \left(\frac{L_w}{H_w} \right)^2 \\ 1 - \alpha_{b1} = 0.56509 \left(\frac{L_w}{H_w} \right)^{-1} + 0.1287 \left(\frac{L_w}{H_w} \right)^{0.5} \\ \alpha_{c2} = 0.1025 \left(\frac{L_w}{H_w} \right)^{-0.5} + 0.046736 \left(\frac{L_w}{H_w} \right)^{0.5} e^{(L_w/H_w)^{-0.5}} \\ 1 - \alpha_{b2} = 0.312751 \left(\frac{L_w}{H_w} \right)^{-1.5} + 0.467931 \left(\frac{L_w}{H_w} \right)^{0.5} \end{array} \right. \quad (16)$$

4 Three-strut model

Saneinejad et al. [Saneinejad and Brain (1995)] proposed a three-strut model based on the stress distribution of ultimate loading state, as shown in Fig. 2.

The shear capacity of the infilled panel in the ultimate loading state can be obtained by:

$$F_w = \sigma_c t_w (1 - \alpha_c) \alpha_c H_w + \tau_b t_w \alpha_b L_w \quad (17)$$

where W is the normalized contact length, and the subscript c and b denote column and beam respectively; W is the normal stress on the contact surface between the column and the panel; W is the shear stress on the contact surface between the column and the panel. W and W can be obtained by:

$$\sigma_c = \frac{f_m}{\sqrt{1 + 3\mu^2 r^4}} \quad (18)$$

$$\tau_c = \mu r^2 \sigma_c \quad (19)$$

where f_m is the compressive bearing capacity of the infill masonry; r is the ratio of infill panel height H_w to length L_w ; W is the friction coefficient of the interface between frame and infill panel. Then the area of equivalent strut A can be obtained by:

$$A = \frac{F_w}{f_m} \quad (20)$$

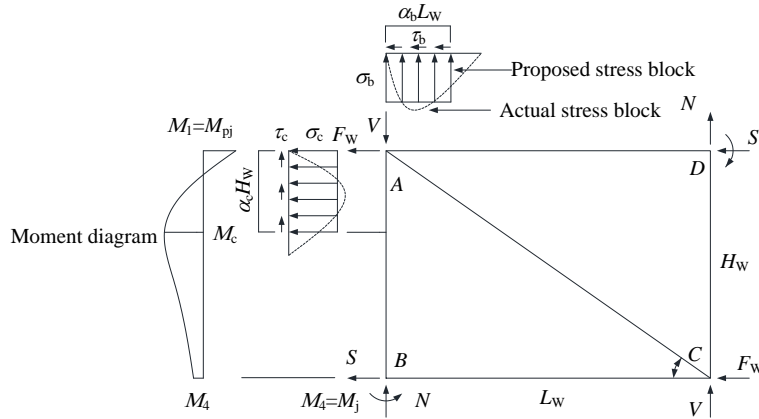


Figure 2: Frame force diagram

A three-strut model considering the contact length between the frame and the infilled panel is built as shown in Fig. 3.

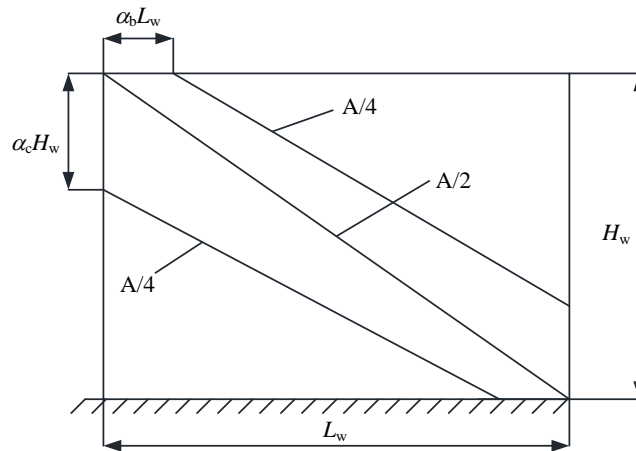


Figure 3: Three-strut model

The contact length between frame and infill panel can be obtained by:

$$\alpha_c H_w = \sqrt{\frac{2(M_{pj} + M_c)}{\sigma_c t_w}} \leq 0.4 \tag{21}$$

$$\alpha_b L_w = \sqrt{\frac{2(M_{pj} + M_b)}{\sigma_b t_w}} \leq 0.4 \tag{22}$$

where M_{pj} is the least of the column, the beam and their joint plastic resist moment; M_b and M_c are the plastic resist moment of the beam and the column respectively; $\bar{\sigma}$ is the normal stress on the contact surface between the beam and the panel, which can be obtain by:

$$\sigma_b = \frac{f_m}{\sqrt{1+3\mu^2}} \tag{23}$$

5 Case study

5.1 Analytical model

The building is an 8-story with the story-height of 3 m. The plane layout of structure is shown in Fig. 4. The infill panels with thickness of 190 mm are made of MU10 ordinary brick block and M5 cement mortar. The cubic compressive strength of concrete is 30 MPa, and the yielding strength of longitudinal reinforcement and stirrup reinforcement are 335 MPa and 300 MPa respectively.

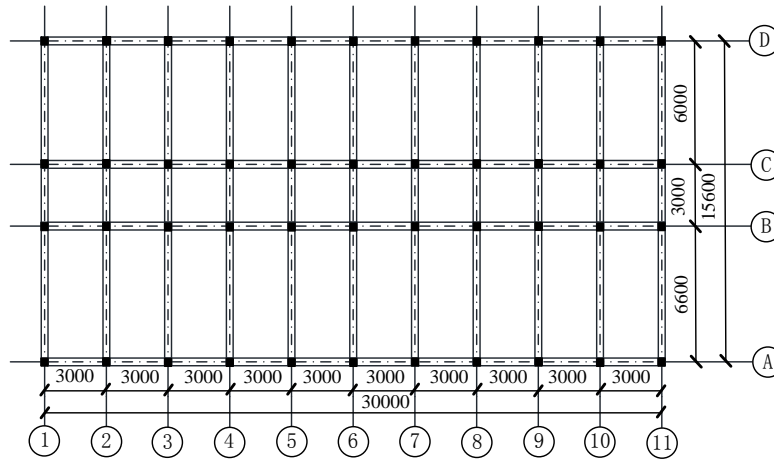


Figure 4: Plane layout of frame

The geometric dimension and reinforcement area of RC components are listed in Tab. 1. and Tab. 2 respectively. The building locates in a region with seismic fortification intensity of 8, seismic design group of 2 and site soil type of 2. Thus, the site characteristic period is 0.4s, and the design ground acceleration corresponding to basic earthquake is 0.2 g.

Table 1: Geometry dimension of beam and column

Floor number	Column (mm)	Beam (mm)	
	Middle and side column	Middle bay	Side bay
1	450×450	200×500	200×650
2-4	450×450	200×500	200×650
5-6	450×450	200×500	200×650
7-8	450×450	200×500	200×650

Table 2: Area of longitudinal reinforcement

Floor number	Column (mm ²)		Beam (mm ²)			
	Middle column	Side column	Middle bay		Side bay	
			Top	Bottom	Top	Bottom
1	2704	3456	1649	1074	1649	1074
2-4	2513	2208	1649	1074	1649	1074
5-6	2032	2032	1257	509	1257	763
7-8	2032	2032	823	509	823	509

The uniaxial stiffness of the equivalent strut calculated according to the models proposed by Tong, FEMA and Saneinejad respectively is listed in Tab. 3.

As shown in the table, the uniaxial stiffness calculated according to Tong's model is significantly higher than the values obtained by the other two models and is considered to be unreasonable. Therefore, the Saneinejad model and FEMA model were used to simulate the infill panel in the following Analysis.

Table 3: Uniaxial stiffness of equivalent strut

model	1 Floor			2-4 Floor			5-6 Floor			7-8 Floor		
	6 m	3 m	6.6 m	6 m	3 m	6.6 m	6 m	3 m	6.6 m	6 m	3 m	6.6 m
Tong	324	129	364	375	140	421	375	140	421	375	140	421
FEMA	61	59	61	64	60	64	64	60	64	64	60	64
Saneinejad	51	98	45	46	100	39	43	83	38	41	83	36

5.2 Numerical model

Pushover and model analysis are carried out on three different models with the software SAP 2000. Two of the models are infilled frames with the panel simulated by FEMA model and Saneinejad model respectively. The other model is bare frame model.

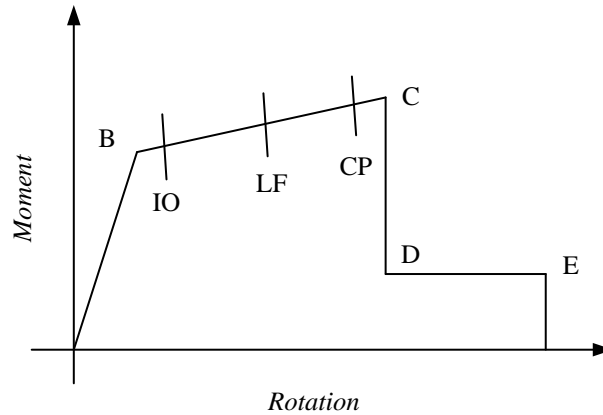


Figure 5: Moment-rotation skeleton curve of lumped plastic hinge

The GAP element bearing pressure only is used to simulate the equivalent strut. M3 moment lumped hinge model and PMM axial-moment lumped hinge model are used to simulate the nonlinear behavior of beam and column respectively. The typical moment-rotation skeleton curve of lumped plastic hinge is shown in Fig.5. The points B and C represent that the plastic hinges reach the plastic state and the ultimate bearing capacity state respectively. The points IO, LF and CP represent that plastic hinges reach Immediate Occupancy, Life Safety and Collapse Prevent performance state respectively. The inverted triangle load mode is adopted to apply load. The capacity spectrum method is adopted in the analysis.

5.3 Results of the analyses

5.3.1 Modal analysis

The first order periods of three models are present in Tab. 4:

Table 4: First order period of the models

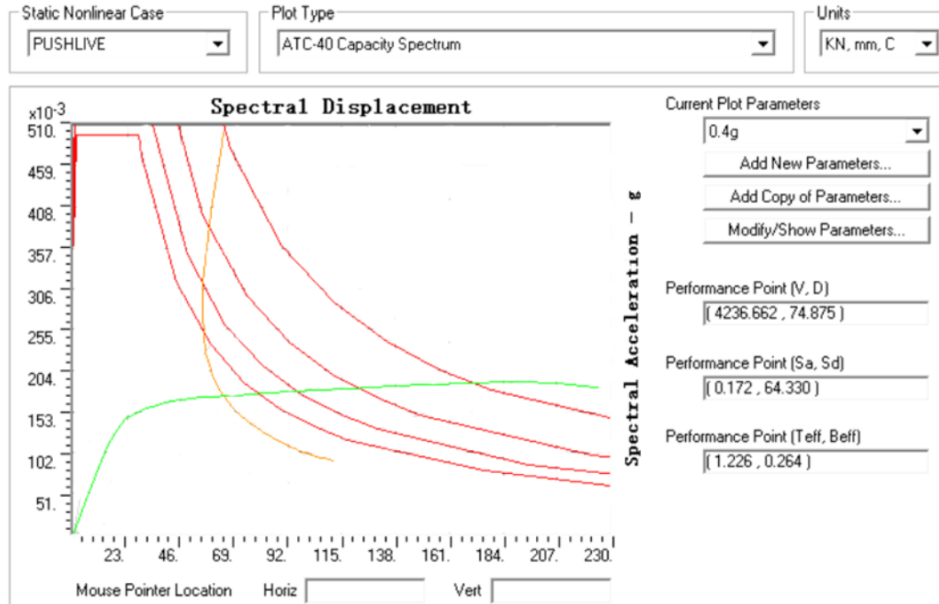
model	Bare frame	FEMA	Saneinejad
Period (s)	0.75	0.33	0.48

As can be seen from the Tab. 4, the period reduction factors (defined as the ratio of the period of infilled frame to the period of bare frame) of FEMA model and Saneinejad model are 0.6 and 0.67 respectively. Compared with the value (0.6-0.7) proposed by current code of Technical specification for concrete structure of high rise building [JGJ3-2010], the period calculated by the model proposed by Saneinejad is closer.

5.3.2 Pushover analysis

When the peak ground acceleration under the maximum considered earthquake is 0.4 g, the capacity spectrums of bare frame model, FEMA model and Saneinejad model are shown in Fig. 6, in which the green curve represents the capacity spectrum and the red curve represents the demand spectrum. The performance points of bare frame model,

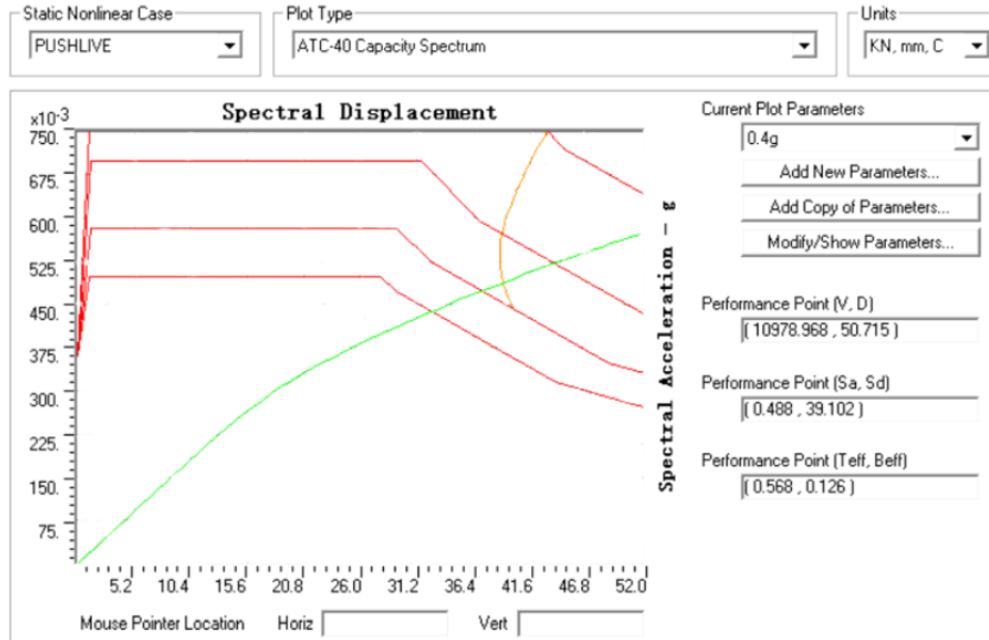
FEMA model and Saneinejad model is 4236.662 KN, 74.875 mm), (9360.339 KN, 30.655 mm) and (10978.968 KN, 50.715 mm) respectively.



(a) Bare frame



(b) FEMA



(c) Saneinejad

Figure 6: Capacity and demand spectrums of three models

The inter-story drifts corresponding to the performance point are listed in Tab. 5.

Table 5: Inter-story drift of three models

Model	1st floor	2st floor	3st floor	4st floor	5st floor	6st floor	7st floor	8st floor
Bare frame	1/233	1/156	1/142	1/245	1/407	1/774	1/1678	1/3115
FEMA	1/750	1/566	1/608	1/646	1/718	1/844	1/1114	1/1678
Saneinejad	1/420	1/337	1/375	1/419	1/444	1/523	1/695	1/1066

The maximum inter-story drift of the bare frame model, FEMA model and Saneinejad model are 1/142 (drift ratio of the third floor), 1/566 (drift ratio of the second floor) and 1/337 (drift ratio of the second floor) respectively, which indicates that the infilled panels can reduce the maximum inter-story drift and change the weak position of the structure.

The distribution of plastic hinge when the three models reach the performance point is shown in Fig. 7. For the bare frame, the plastic hinge at column bottom of the first and second floor enters plastic state, and the plastic hinge at the beam end of most of the floor reaches the IO performance state. For the frame with infill wall, the amount of IO plastic hinge at beam end significantly reduced, while more plastic hinges occurred at the top and bottom of the column in the second and third floor. It is indicated that the infill wall significantly reduces the damage of the beam, and increase the damage of column.

According to the “strong column and weak beam” design philosophy, the influence of the infilled wall on the seismic performance of the structure is unfavorable.

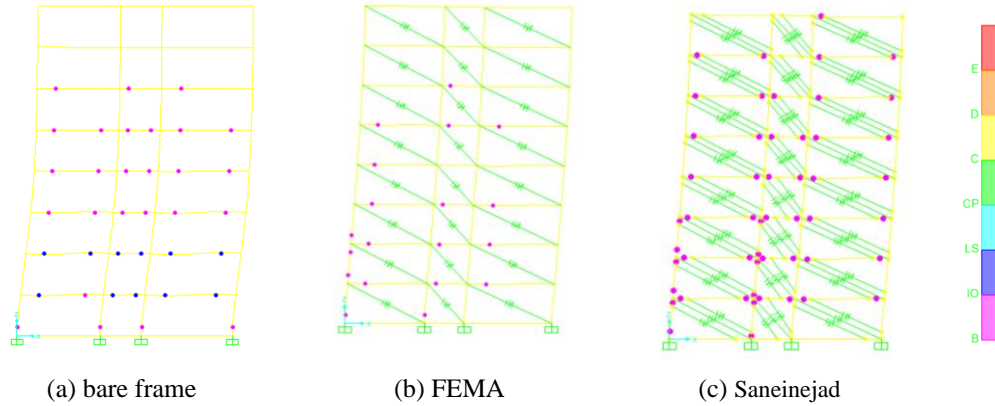
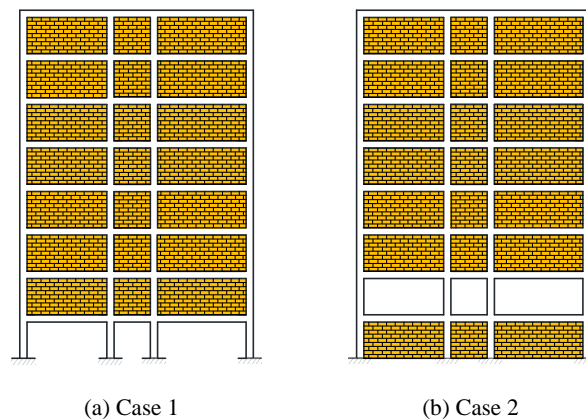


Figure 7: Distribution of plastic hinge (PGA=0.4 g)

6 Influence of the irregular configuration of infill walls

In order to study the influence of the configuration of infill walls on the aseismic performance of infilled frames, pushover analysis is carried out on 5 infilled frames with different configuration of infill walls as shown in Fig. 8.

The capacity and demand spectrums of five kinds of infilled frames with different types of arrangement under the earthquake with a peak ground acceleration of 0.4 g are shown in Fig. 9, and the performance points are listed in Tab. 6. The calculate results of Case 1, Case 4 and Case 5 indicated that the base shear force and roof displacement of the infilled frame increase with the increasing of the number of infill walls. This is because the infill wall can bear a part of horizontal force and can improve the lateral stiffness of infilled frame. The calculate results of Case 1, Case 2 and Case 3 indicated that position of the single unfilled story has a negligible effect on the base shear force.



(a) Case 1

(b) Case 2

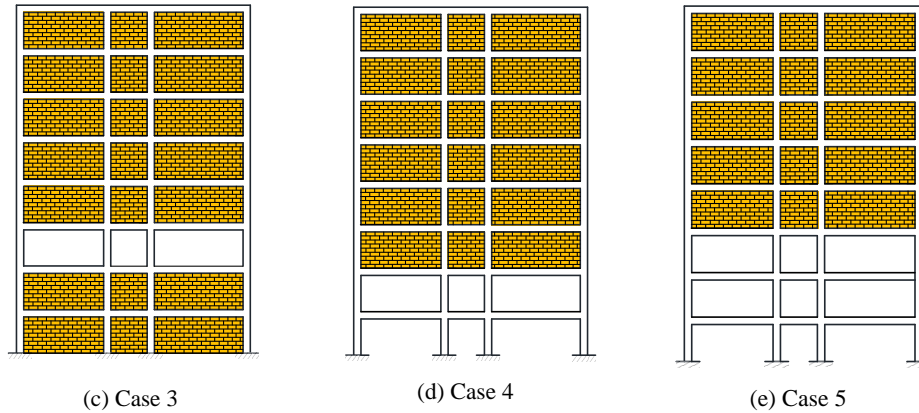


Figure 8: Configuration of infill walls

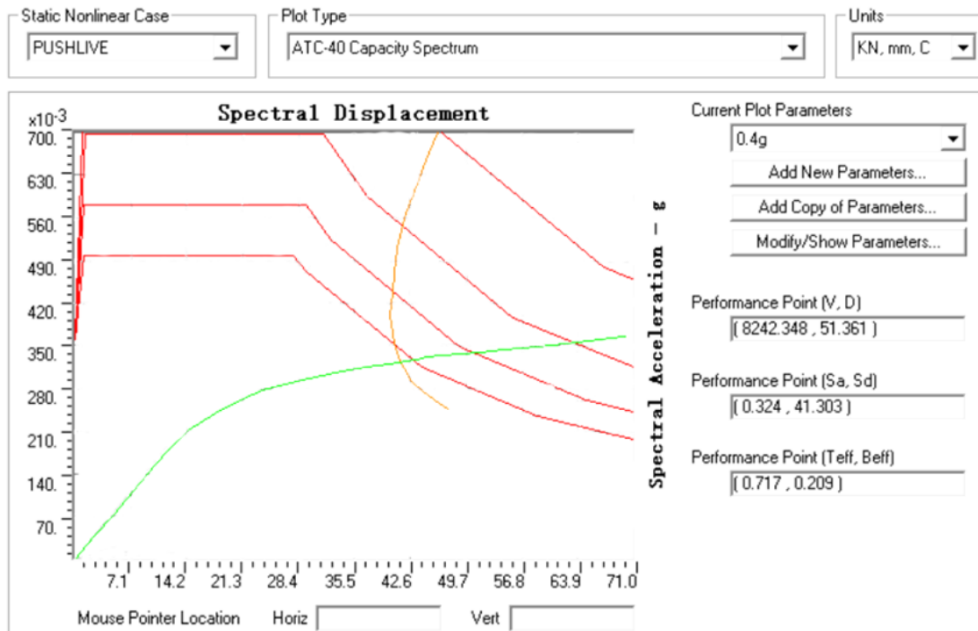
Table 6: Performance points of infilled frame for five case (PGA=0.4 g)

Model	Case 1	Case 2	Case 3	Case 4	Case 5
Base shear force (kN)	8242.3	7003.491	7175.096	5202.778	4475.378
Roof displacement(mm)	51.36	50.760	48.536	60.651	66.675

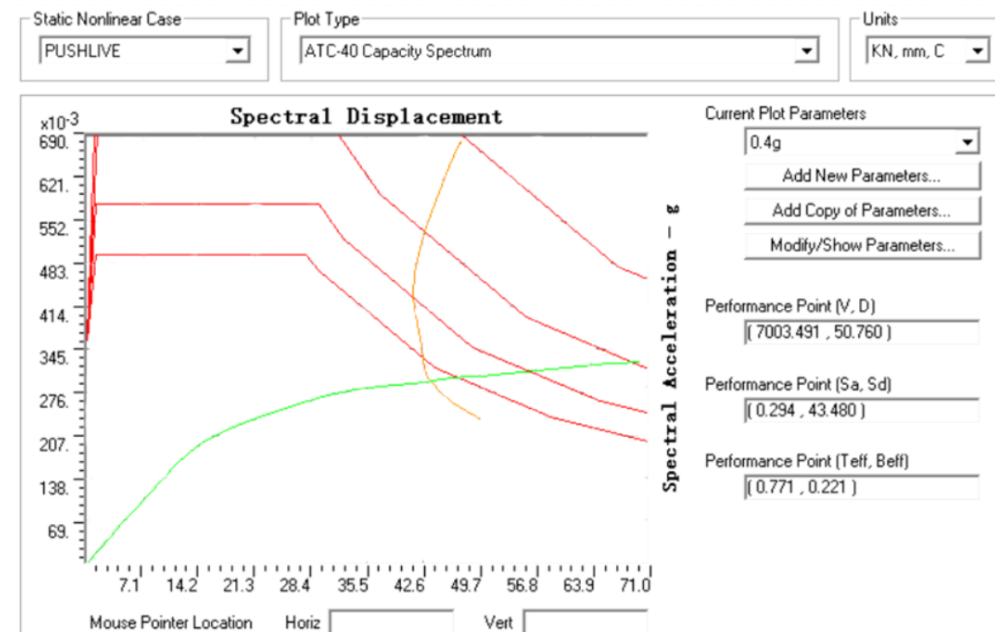
The inter-story drifts of the infilled frames when frames reach the performance points are list in Tab. 7. It can be observed that the inter-story drift of the unfilled story is significantly larger than that of infilled story, which means the unfilled story is the weak position of infilled frame. The maximum inter-story drift of the five case are close, which means in a certain condition, the position of single unfilled story and the number of unfilled stories at the bottom of the structure have a negligible effect on the maximum inter-story drift of infilled frame.

Table 7: Inter-story drift of infilled frame for five cases

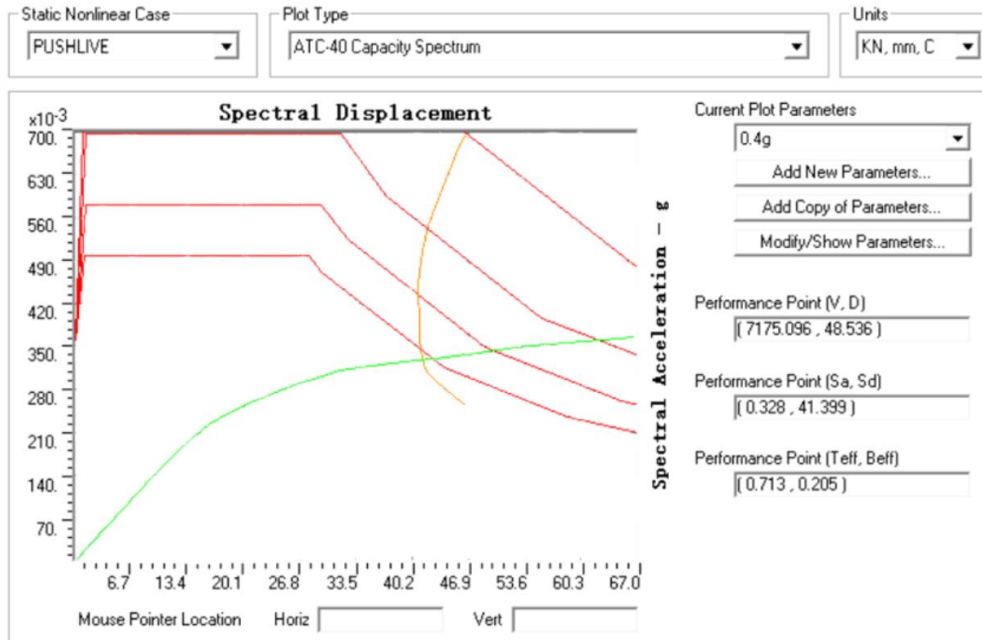
Model	1st floor	2st floor	3st floor	4st floor	5st floor	6st floor	7st floor	8st floor
Case 1	1/151	1/414	1/509	1/612	1/652	1/762	1/997	1/1490
Case 2	1/505	1/128	1/507	1/765	1/819	1/950	1/1215	1/1765
Case 3	1/823	1/513	1/138	1/551	1/812	1/948	1/1220	1/1801
Case 4	1/141	1/128	1/723	1/1043	1/1143	1/1327	1/1690	1/2427
Case 5	1/190	1/136	1/161	1/973	1/1366	1/1601	1/2030	1/2959



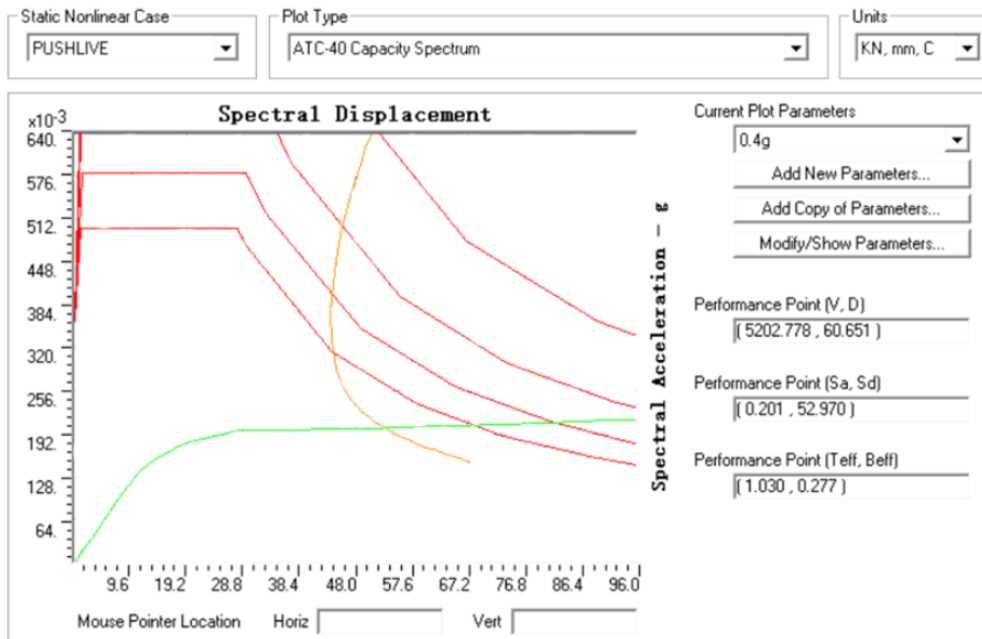
(a) Case 1



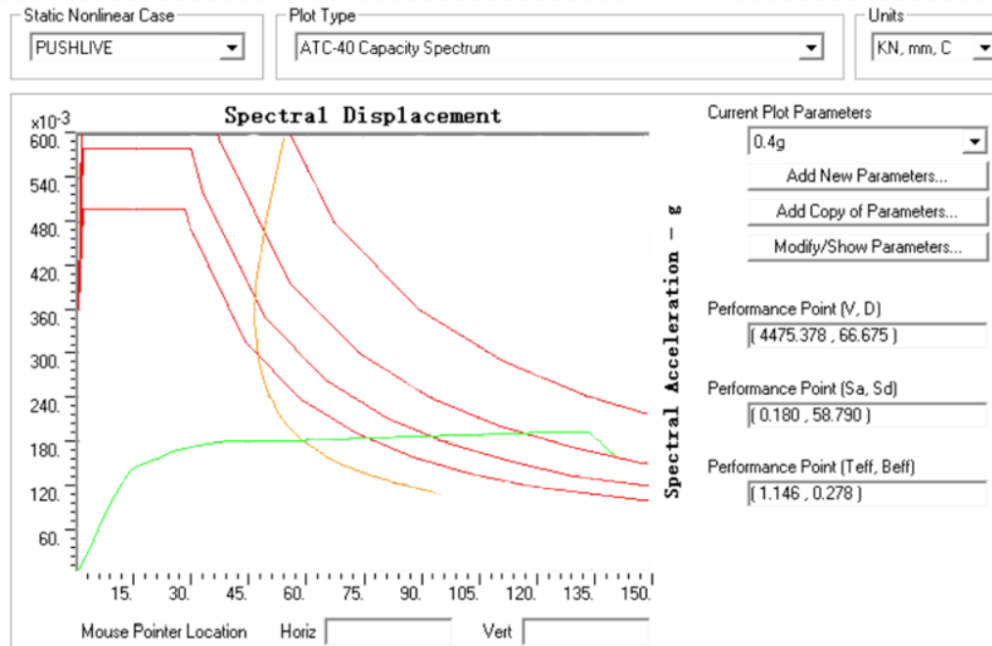
(b) Case 2



(c) Case 3



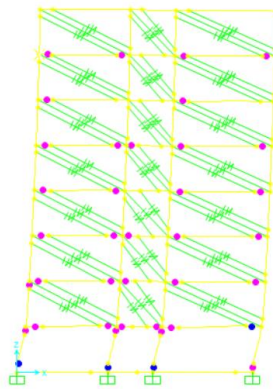
(d) Case 4



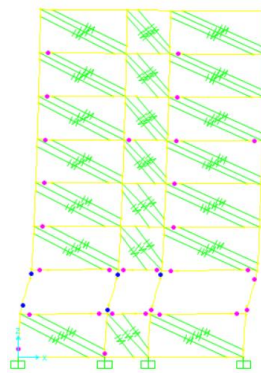
(e) Case 5

Figure 9: Capacity and demand spectrums of five cases

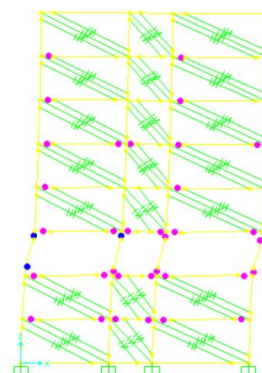
When the infilled frame reaches the performance point, the distribution of plastic hinge of the frame is shown in Fig. 10, it can be observed that the damage degree of unfilled story is higher than the infilled story, which further indicate that the unfilled story is the weak position of frame. This weak story may cause collapse of the structure in the earthquake.



(a) Case 1



(b) Case 2



(c) Case 3

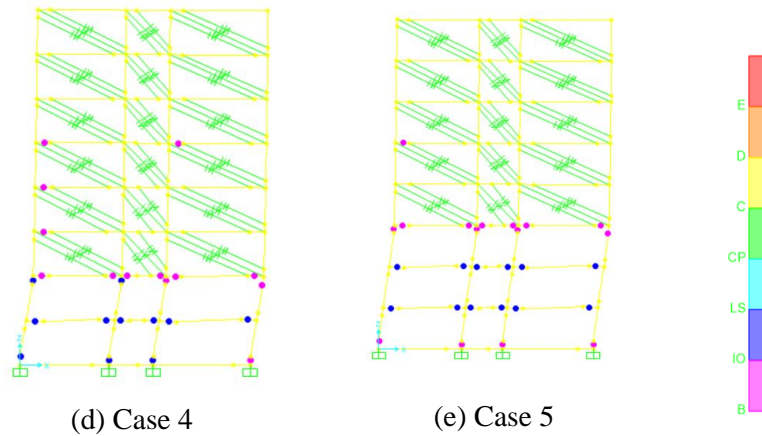


Figure 10: Distribution of plastic hinge for five cases (PGA=0.4 g)

By comparing the plastic hinge distribution of Case 1, Case 4 and Case 5, it can be seen that when the unfilled story at the bottom of infilled frame, the seismic response of the upper fill layer decreases with the increasing of the number of unfilled stories.

7 Conclusions

- (1) In comparing with the period of the infilled frame based on the equivalent single strut model, the period of the infilled frame based on equivalent three-strut model is closer to the value recommended by the current Chinese code.
- (2) The stiffness and the bearing capacity of the infilled frame increases with the increasing of the number of the infill walls.
- (3) The existence of infilled wall can change the weak position of the structure, and may lead to the unfavorable failure mechanism of the frame, which should be paid attention.
- (4) When the infill wall is discontinuously arranged along the vertical direction of the infilled frame, the unfilled story is the weak position of infilled frame, and when the unfilled story at the bottom of infilled frame, the seismic response of the upper fill layer decreases with the increasing of the number of unfilled stories.
- (5) There are some shortcomings in the existing model. Firstly, the influence of opening on the infilled wall is not considered. Secondly, the influence of infilled panel on the out-of-plane seismic performance of frame is not considered. The model considering these factors should be built in the future.

Acknowledgements: This research is supported by Natural Science Foundation of Fujian Province, China (Grant No. 2015J01212).

References

- Asteris, P. G.; Cotsovos, D. M.; Chrysostomou, C.; Mohebkahd, A.; Al-Chaare, G. K.** (2013): Mathematical micromodeling of infilled frames: state of the art. *Engineering Structures*, vol. 56, pp. 1905-1921.
- Basha, S. H.; Kaushik, H. B.** (2016): Behavior and failure mechanism of masonry-infilled RC frames (in low-rise buildings) subject to lateral loading. *Engineering Structures*, vol. 111, pp. 233-245.
- Crisafulli, F. J.; Carr, A.; Park, R.** (2000): Analytical modelling of infilled frame structures-A general review. *Bulletin of the New Zealand Society for Earthquake Engineering*, vol. 33, no. 1, pp. 30-47.
- Cavaleri, L.; Trapani, F. D.** (2014): Cyclic response of masonry infilled RC frames: Experimental results and simplified modeling. *Soil Dynamic and Earthquake Engineering*, vol. 65, pp. 224-242.
- Chiou, T.; Hwang, S.** (2015): Tests on cyclic behavior of reinforced concrete frames with brick infill. *Earthquake Engineering and Structural Dynamics*, vol. 44, no. 12, pp. 1939-1958.
- De Luca, F.; Verderame, G. M.; Gomez-Martinez, F.** (2014): The structural role played by masonry infills on RC building performances after the 2011 Lorca, Spain, earthquake. *Bulletin of Earthquake Engineering*, vol. 12, no. 5, pp. 1999-2026.
- Dakhakhni, W. W.; Elgaaly, M.; Hamid, A. A.** (2003): Three-strut model for concrete masonry-infilled steel frames. *Journal of Structural Engineering*, vol. 129, no. 2, pp. 177-185.
- FEMA; ASCE** (1997): *FEMA 273 NEHRP Guidelines for the Seismic Rehabilitation of Buildings*. Federal Management Emergency Agency, pp. 7-18.
- FEMA; ASCE** (2000): *FEMA 356 Prestandard and Commentary for the Seismic Rehabilitation of Buildings*. Federal Emergency Management Agency, pp. 7-25.
- Fiore, A.; Netti, A.; Monaco, P.** (2012): The influence of masonry infill on the seismic behavior of RC frame buildings. *Engineering Structures*, vol. 44, no. 6, pp. 133-145.
- Furtado, A.; Rodrigues, A.; Arede A.; Varum, H.** (2015): Influence of the in plane and out-of-plane masonry infill wall's interaction in the structural response of RC building. *Procedia Engineering*, vol. 114, pp. 722-729.
- Furtado, A.; Rodrigues, H.; Arede A.** (2015): Modelling of masonry infilled walls participation in the seismic behavior of RC buildings using OpenSees. *International Journal of Advanced Structural Engineering*, vol. 7, no. 2, pp. 117-127.
- Huang, Q. X.** (2011): *Study on Seismic Behavior and Elastic-Plastic Analysis Method for Seismic Response of RC Frame Infilled with New Masonry (Ph.D. Thesis)*. National Huaqiao University.
- Guo, Z. X.; Huang, Q. X.; Wei, R. F.; Liu, L.** (2009): Experimental study on seismic behavior of RC frames with slab and infilled masonry walls. *Journal of Building Structures*, vol. S2, pp. 127-132.
- Holmes, M.** (1961): Steel frames with brickwork and concrete infilling. *Proceedings of the Institution of Civil Engineers*, vol. 19, no. 6501, pp. 48-60.

- Karayannis, C. G.; Favvate, M. J.; Kakavetsis, D. J.** (2011): Seismic behavior of infilled and pilotis RC frame structures with beam-column joint degradation effect. *Journal of Structural Engineering*, vol. 33, no. 10, pp. 2821-2831.
- Koutromanos, I.; Stavridis, A. M.; Shing, P. S.; Willam, K.** (2011): Numerical modeling of masonry-infilled RC frames subjected to seismic loads. *Computers & Structures*, vol. 89, no. 11-12, pp. 1026-1037.
- Mallick, D. V.; Severn, R. T.** (1967): The behavior of infilled frames under static loading. *Proceedings of the Institution of Civil Engineers transportation*, vol. 11, pp. 69-102.
- Mehrabi, A. B.; Shing, P. B.** (2002): Behaviour and analysis of masonry-infilled frames. *Progress in Structural Engineering and Materials*, vol. 4, no. 3, pp. 320-331.
- Ministry of Housing; Urban-Rural Development of People's Republic of China** (2010): *JGJ3-2010 Technical Specification for Concrete Structure of High Rise Building*. China Construction Industry Press, Beijing.
- Moaveni, B.; Stavridis, A.; Lombaert, G.; Conte, J. P.; Shing, P. B.** (2013): Finite-element model updating for assessment of progressive damage in a 3-story infilled FC frame. *Journal of Structural Engineering*, vol. 139, no. 10, pp. 1665-1674.
- Moretti, M. L.; Mousafiroopoulos, G.; Fotakopoulos, T.; Makarios, T. K.** (2013): Influence of masonry infills in torsional irregular RC buildings. Part 2: Analysis and results according to the Eurocodes. *World Congress on Advances in Structural Engineering and Mechanics*, pp. 1752-1761.
- Mulgund, G. V.; Kullkarni, A. B.** (2011): Seismic assessment of RC frame buildings with brick masonry infills. *International Journal of Advanced Engineering Sciences and Technologies*, vol. 2, pp. 140-147.
- Puglisi, M.; Uzcategui, M.; Florez-Lopez, J.** (2009): Modeling of masonry of infilled frames, Part II: Cracking and damage. *Engineering Structures*, vol. 31, pp. 119-124.
- Pujol, S.; Fick, D.** (2010): The test of a full-scale three-story RC structure with masonry infill walls. *Engineering Structures*, vol. 32, pp. 3112-3121.
- Saneinejad, A.; Brain, H.** (1995): Inelastic design of infill frames. *Journal of Structural Engineering*, vol. 121, no. 4, pp. 634-650.
- Smith, B. S.** (1966): Behavior of square infilled frames. *Journal of the Structure Division*, vol. 92, no. 1, pp. 381-404.
- Tasnimi, A. A.; Mohebkah, A.** (2011): Investigation on the behavior of brick-infilled steel frames with openings, experimental and analytical approaches. *Engineering Structures*, vol. 33, pp. 968-980.
- Tong, Y. S.; Qian, G. F.; Liang, X. W.; Guo, B. H.** (1985): Stiffness of RC frame with brick infilled wall and its application. *Journal of Metallurgy and Architecture Institute*, vol. 44, no. 4, pp. 21-35.
- Yuen, Y. P.; Kuang, J. S.** (2015): Nonlinear seismic response and lateral force transfer mechanisms of RC frames with different infill configurations. *Engineering Structures*, vol. 91, pp. 125-140.